

# pH-dependent dissociation from CTLA-4 in early endosomes improves both safety and antitumor activity of anti-CTLA-4 antibodies

Meiyu Zhang<sup>a,1</sup>, Jinmei Lia<sup>1</sup>, Kepeng Yan<sup>a,1</sup>, Haoyue Zhou<sup>a</sup>, Song Mei<sup>a</sup>, Benyu Wang<sup>a</sup>, Dongyang Li<sup>a</sup>, Xuexiang Du<sup>b,c</sup>, Mingyue Liu<sup>b,d</sup>, Peng Zhang<sup>e</sup> 🗓, James K. Fields<sup>b,f</sup>, Lei Ye<sup>g,h</sup>, Pan Zheng<sup>b,i</sup>, Yang Liu<sup>b,i</sup>, Michael J. Lenardo<sup>j,2,3</sup>, and Yan Zhang<sup>a,k,2</sup>

Affiliations are included on p. 10.

Contributed by Michael J. Lenardo; received November 1, 2024; accepted January 13, 2025; reviewed by Kenneth M. Murphy and Jenny Ting

Anti-CTLA-4 Abs (ACAs) are a breakthrough for cancer therapy, but their potential is limited by immunotherapy-related adverse events (irAE). We previously reported that ACAs with acidic pH-sensitive binding to CTLA-4 exhibit higher antitumor activity with fewer irAE. We now test a panel of variants of Ipilimumab (Ipi), the first ACA cancer therapeutic, for tumoricidal efficacy and irAE. Surprisingly, not all pH-sensitive Ipi variants exhibited an enhanced therapeutic index. Ipi13, which retained binding to CTLA-4 at pH 6.0 but dissociated at lower pH, showed no enhancement. By contrast, Ipi25, which dissociates from CTLA-4 at pH 6.0, the pH of the early endosome (EE), showed greater tumor regression and less severe irAE. Confocal microscopy showed that Ipi13 maintained colocalization with CTLA-4 at the late endosomes (LE) and lysosomes resulting in lysosomal degradation of CTLA-4. Conversely, Ipi25 did not colocalize with CTLA-4 in LE or lysosomes after endocytosis but allowed both proteins to transfer to recycling endosomes. EE dissociation was also characteristic of variants of Tremelimumab (Treme), another clinical ACA, that showed better efficacy and fewer side effects. Thus, our data reveal the significance of early intracellular dissociation from CTLA-4 to improve ACAs for safer and more effective cancer immunotherapy.

CTLA-4 | immunotherapy | intracellular trafficking | Rabs

A major challenge in cancer immunotherapy, specifically in targeting CTLA-4, is to decrease immunotherapy-related adverse events (irAE) without significantly impeding therapeutic efficacy (1-3). Antitumor activity and irAE are both triggered by anti-CTLA-4 mAbs (ACAs) binding to CTLA-4 (4-6). CTLA-4 is a cell surface protein that binds CD80 and CD86 on antigen-presenting cells (7–9), to inhibit T cell responses. Mutations of the Ctla4 gene lead to autoimmune diseases in the mouse and human (10–15). Similar types of autoimmunity are observed as irAE in patients treated with ACA for cancer immunotherapy (5, 16, 17). These irAE cause significant morbidity and mortality and limit the doses and duration of ACA therapy (18, 19).

Recent studies, including our own, have shown in preclinical tumor models that the irAE and antitumor activity of ACA may be mediated by distinct mechanisms (20-22). The antitumor effect of ACA may primarily involve selective depletion of CD4<sup>+</sup>, FoxP3<sup>+</sup> regulatory T cells in the tumor microenvironment (TME) through the activation of Fc receptor (FcR)-dependent antibody-dependent cell-mediated cytotoxicity (ADCC) or antibody-dependent cellular phagocytosis (ADCP) (21, 23-25). Higher expression of CTLA-4 on tumor-associated Tregs and increased numbers of FcyRIII-IV-positive tumor-associated macrophages/monocytes have both been proposed as mechanisms underlying tumor-specific Treg depletion (20, 21, 26, 27). On the other hand, ACA-induced irAE are likely through a different activity of ACA. CTLA-4 is constantly endocytosed and recycled between the cell surface and endosomes and protected from lysosomal degradation by binding to LRBA (the lipopolysaccharide-responsive and beige-like anchor) (13–15). Clinical ACA hinder CTLA-4 recycling by staying bound to CTLA-4 postendocytosis and impeding association with LRBA (28). Therefore, irAE are attributable to lysosomal degradation of ACA:CTLA-4 complexes after ACA-mediated disruption of CTLA-4 recycling thereby eliminating CTLA-4 expression on T lymphocyte populations (28).

We have reported that the pH sensitivity of ACA binding to CTLA-4 is a key factor affecting the incidence and severity of irAE as well as antitumor activity (28). Upon binding to cell surface CTLA-4, the ACA:CTLA-4 complex undergoes internalization and enters a series of intracellular compartments characterized by progressively lower

# **Significance**

A major challenge in cancer immunotherapy is to reduce immunotherapy-related adverse events (irAE) while improving therapeutic efficacy. Our work reveals how early endosome (EE) pH 6.0 sensitivity affects the intracellular trafficking of anti-cytotoxic T-lymphocyteassociated protein 4 (CTLA)-4 mAb (ACA) and CTLA-4 and the therapeutic indices of ACA. This insight provides an approach to generate safer and more effective ACA. Since antibody-induced endocytosis occurs often in immunotherapy, our study suggests fine-tuning pH sensitivity to alter the intracellular trafficking of both targets and antibodies as a valuable avenue to engineer better therapeutic antibodies. Taken together, our data indicate that transforming a pH-insensitive ACA into an EE pH 6.0-sensitive ACA may represent a potentially universal principle for engineering safer and more effective ACA therapy.

Competing interest statement: P. Zheng and Y.L. are co-founders and have equity interest in OncoC4. Other authors declare no competing interests. Patent application submitted on antibody variants

Copyright © 2025 the Author(s). Published by PNAS. This article is distributed under Creative Commons Attribution-NonCommercial-NoDerivatives License 4.0 (CC BY-NC-ND).

<sup>1</sup>M.Z., J.L., and K.Y. contributed equally to this work.

<sup>2</sup>To whom correspondence may be addressed. Email: lenardo@nih.gov or zhy3331a@shsmu.edu.cn.

<sup>3</sup>Present address: Calico Life Sciences, Limited Liability Company, South San Francisco, CA 94080

This article contains supporting information online at https://www.pnas.org/lookup/suppl/doi:10.1073/pnas. 2422731122/-/DCSupplemental.

Published February 18, 2025

internal pH compared to the extracellular environment. Ipilimumab (Ipi) and Tremelimumab (Treme), two ACAs widely used in cancer therapy, have been shown to exhibit stable binding to CTLA-4 at low pH (28). Upon binding to CTLA-4 on the cell membrane, they are internalized into the cell along with CTLA-4. Their strong binding to CTLA-4 at low pH prevents the recycling of CTLA-4, leading the ACA:CTLA-4 complex to be directed to lysosomes (pH 4.5) for degradation (28). The sustained degradative loss of CTLA-4 leads to the irAEs (10, 28, 29). By contrast, we have shown that ACAs that lose binding at acidic pH allow CTLA-4 to avoid lysosomal degradation and recycle back to the PM to promote immunological tolerance and prevent irAE (28). We therefore tested a series of pH-sensitive Ipi variants to evaluate the specific pH requirements for improved therapeutic indices.

#### **Results**

Site-Directed Tyr→His Mutations in CDRs (Complementary-Determining Regions) Yield Two Distinct Groups of Ipi Variants. We previously demonstrated that targeted substitutions of His for specific tyrosine (Tyr) residues in the CDRs of Treme altered the pH sensitivity of binding to CTLA-4 (28, 30). Based on these data, we generated a panel of Ipi variants with Tyr to His substitutions in two tyrosine residues in the light chain CDRs and four tyrosine residues in the heavy chain CDRs, resulting in a total of 23 different genetic variants of Ipi (Fig. 1A and SI Appendix, Fig. S1A and Tables S1 and S2). We next measured binding to plate-bound CTLA-4 across a pH range from 4.5 to 7.0 (SI Appendix, Fig. S1 B–E). HL12, a pH-sensitive ACA with a desirable therapeutic index served as a control (28). Among the five variants with mutations solely in the heavy chain CDRs (Ipi01-05), we found that three variants (Ipi02, Ipi04, and Ipi05) bound similarly to Ipi, whereas Ipi01 and Ipi03 showed reduced binding only at pH 4.5 (SI Appendix, Fig. S1B). Since pH 4.5 is characteristic of the lysosome, releasing CTLA-4 at this pH would not prevent CTLA-4 degradation. We next generated Ipi variants with mutations in both heavy and light chains. We found that when a single His-Tyr replacement in the light chain CDR was combined with different mutations in the heavy chain CDRs, some variants (Ipi11, Ipi12, Ipi15, and Ipi24) bound comparably to Ipi at neutral pH and remained mostly bound to CTLA-4 down to pH 4.5, while other variants, including Ipi13, Ipi14, and Ipi25 exhibited a partial reduction in CTLA-4 binding at neutral pH but showed significant dissociation at varying pH (SI Appendix, Fig. S1 *C* and *D*). Despite this, these variants retained considerable biological activity, as evidenced by their antitumor efficacy in Fig. 1. These mutant antibodies could be divided into two groups. Group 1 (Ipi11, Ipi13, and Ipi14) that lost CTLA-4 binding only at late endosomal (LE) or lysosomal pH, i.e., 4.5 (SI Appendix, Fig. S1C). Group 2 (Ipi21-23, Ipi25) that lost CTLA-4 binding at higher early endosome (EE) pH, i.e., 6.0 (SI Appendix, Fig. S1D). Variants with two His-Tyr replacements in the light chain CDRs combined with heavy chain mutations further enhanced pH sensitivity. However, these variants (Ipi30-35) lost binding to CTLA-4 at all pHs tested (*SI Appendix*, Fig. S1*E*).

Based on these preliminary experiments, we chose Ipi13 and Ipi25 as representatives of Group 1 and Group 2 variants, respectively, and systematically compared them with Ipi. Their binding affinities to CTLA-4 were assessed using the ELISA. As shown in Fig. 1*B*, under neutral pH conditions, both Ipi13 and Ipi25 exhibited decreased binding compared to Ipi, with Ipi25 demonstrating weaker binding than Ipi13. In the pH range of 5.5 to 6.5, Ipi13 and Ipi25 displayed varying degrees of pH-sensitive binding, with Ipi25 showing greater sensitivity than Ipi13. When the pH further

dropped to 4.5 to 5.0, both variants lost binding to CTLA-4 (Fig. 1 *B*, *Left*). Thus, the difference in pH sensitivity between Ipi25 and Ipi13 was in the range of pH 5.5 to 6.5. To clarify this difference, we normalized these data to CTLA-4 binding at pH 7.0 and found that Ipi25 exhibited a greater drop in binding at pH 6.0 compared to Ipi13 using Ipi binding as a baseline (Fig. 1 *B*, *Right*). In contrast, Ipi13 had a smaller drop in binding between pH 7.0 and pH 6.0, but lost binding at pH 5.0 (Fig. 1 *B*). Both mutants had appreciable loss of binding at pH 4.5 and 5.0, whereas Ipi retained substantial binding at these pHs. Thus, while Ipi25 and Ipi13 variants were pH sensitive, their dissociation differed at the EE pH 6.0.

To further quantitate the difference between Ipi13 and Ipi25, we measured the kinetics of binding to CTLA-4 at pH 6.0 and pH 7.4 using surface plasma resonance (SPR), with Ipi as a control (SI Appendix, Fig. S2A). At pH 7.4, although Ipi13 demonstrated a twofold lower affinity (KD) and Ipi25 exhibited a fourfold lower affinity compared to parental Ipi, all had high (subnanomolar) binding affinity to CTLA-4. Interestingly, Ipi showed twofold to threefold increased affinity at 6.0 compared to pH 7.4 due to an increased on-rate  $(k_a)$  and reduced off-rate  $(k_d)$ . We observed twofold to threefold differences in affinity between the variants and Ipi but little difference between Ipi13 and Ipi25, which have essentially the same on-rate and a difference in off-rate that is less than twofold. However, the variants differed in pH sensitivity. Ipi13 showed no difference in affinity at either pH, but Ipi25 had a twofold reduced K<sub>D</sub> at pH 6.0 compared to pH 7.4. This is due to a fourfold lower off-rate which more than offsets a modestly increased on-rate. Therefore, CTLA-4 binding to Ipi and Ipi13 was pH 6.0 insensitive, but Ipi25 was pH 6.0 sensitive. Moreover, Ipi25 has 24-fold lower affinity than Ipi at pH 6.0, primarily due to a sevenfold increase in dissociation constant (kd).

To substantiate these kinetic data, we measured the dissociation of Ipi13, Ipi25, and Ipi from plate-bound CTLA-4 at pH ranging from 4.5 to 7.0. We first allowed all ACAs to bind to CTLA-4 at pH 7.0, followed by a wash to remove unbound antibody. After 2 h of incubation at various low pH levels, the dissociation of the antibody from CTLA-4 was assessed by measuring the change in CTLA-4 binding relative to pH 7.0. As shown in Fig. 1*C* and *SI Appendix*, Fig. S2*B*, at pH 5.5 or lower, both Ipi13 and Ipi25 significantly dissociated, but Ipi remained bound. At pH 6.0 and higher, all antibodies bound, and dissociation at pH 6.0 was observed only for Ipi25 but not Ipi13.

Ipi25 Exhibits an Improved Safety Profile. To first test the biological significance of the distinct pH sensitivity of different Ipi variants, we compared irAE induced by anti-PD-1 mAb in conjunction with ACAs in young Ctla4<sup>h/h</sup> mice (humanized CTLA-4 knock-in mice), an established model for irAE (20). The mice were injected with Ipi or the variants on days 10, 13, 16, and 19 after birth, and their body weight, hematologic changes, and histopathology were evaluated after 30 d. Mice receiving anti-PD-1 in conjunction with either Ipi13 or Ipi showed growth retardation starting at day 12 (Fig. 1D). By contrast, Ipi25-treated mice grew normally. In addition, significant reductions in total hemoglobin (Hb) and blood hematocrit (HCT) were observed when Ipi13 and Ipi, but not Ipi25, were administered (SI Appendix, Fig. S3A). Histological analysis of lymphocyte infiltration as a manifestation of irAE was performed in a double-masked fashion as we have previously reported (20, 28). We found that Ipi13 and Ipi, but not Ipi25, induced severe infiltration in multiple organs (Fig. 1E and SI Appendix, Fig. S3B). These data demonstrated that Ipi25, the pH 6.0-sensitive antibody, had a markedly improved safety profile compared to Ipi.

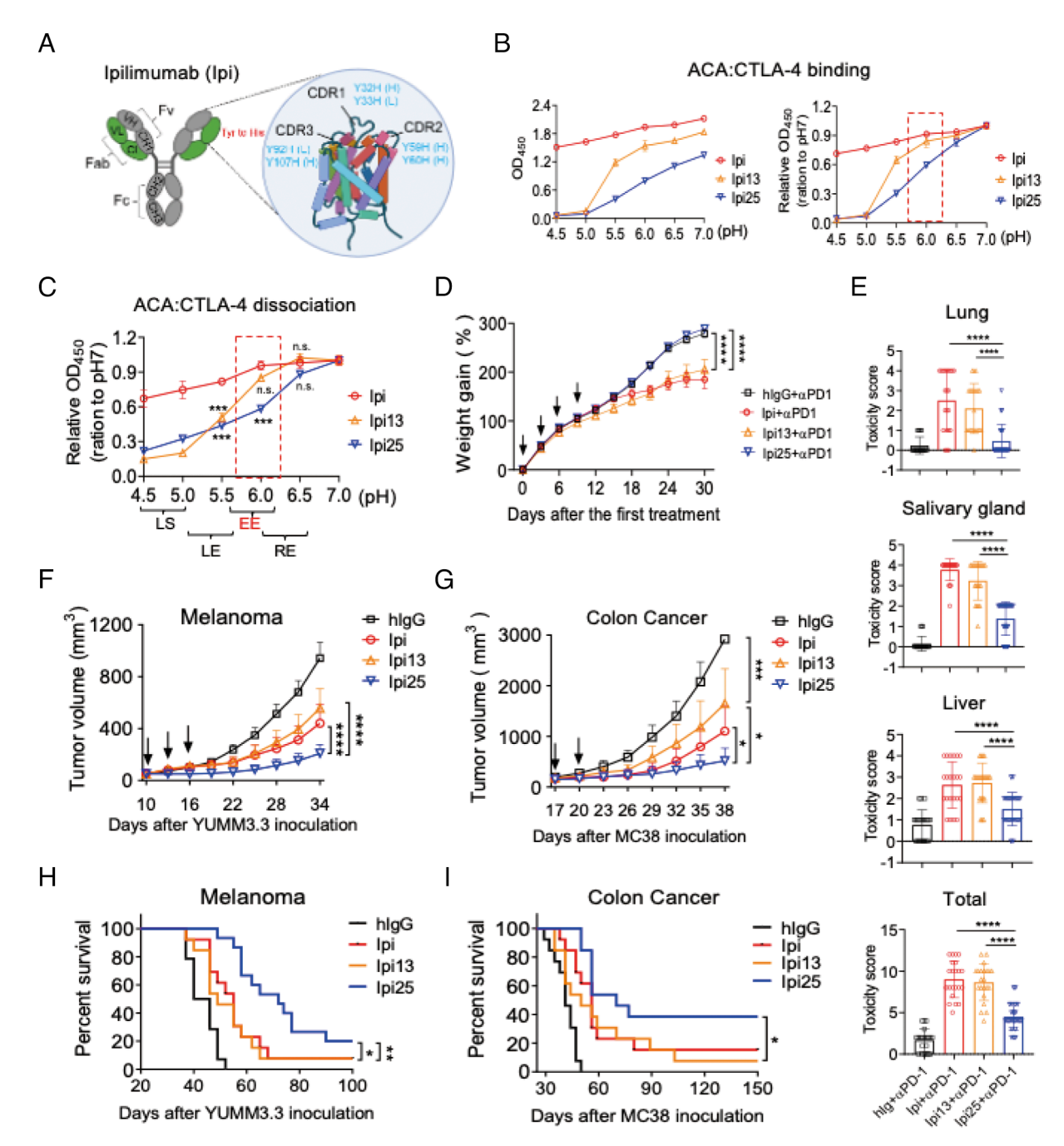


Fig. 1. Engineered pH 6.0 sensitivity improves the safety profile and antitumor activity of Ipi. (A) Schematic Ipi structure showing the Tyr to His amino acid substitutions in the CDRs on both heavy and light chains. Fab: antigen-binding fragment; Fc: crystallizable fragment; Fv: variable fragment; CDR complementarity determining region. (B) ELISA showing the pH dependence of binding of Ipi variants as the optical density at 450 nm (OD<sub>450</sub>) binding of labeled antibody to immobilized hCTLA-4 (Left), and showed as a ratio with the value at pH 7 (Right) for Ipi (red), mutant Ipi13 (orange), and mutant Ipi25 (blue). (C) The pH-sensitive dissociation of the Ipi variants Ipi13 and Ipi25 were examined and shown as duplicate optical density at 450 nm shown as a ratio with the value at pH 7 for Ipi (red), mutant Ipi13 (orange), and mutant Ipi25 (blue). Representative data of two or three independent experiments for (B and C) are shown. (D) Body weight B0 gain (mean  $\pm$  SEM) of 10-d-old C57BL/6 Ctla4B1/m mice injected with 100 B2/m groupe of control hlgG, Ipi, Ipi13, and Ipi25 on days 10, 13, 16, and 19 after birth plus αPD-1. (F) Composite toxicity scores of the organs and glands were determined. The samples were collected from three independent experiments and have been scored double-blind. The bars show means with SE. (F) Tumor volume averages and SEM over time are displayed for YUMM3.3 melanoma tumor-bearing Ctla4<sup>h/h</sup> mice (n = 13 to 14/group) injected intraperitoneally with control hlgG, lpi, lpi13, or lpi25 (30 µg/mouse) on days 10, 13, and 16 after tumor inoculation (indicated by arrows). (G) MC38 tumor-bearing Ctla4hth mice (n = 13/group) were injected i.p. with control hlgG, lpi, lpi13, or lpi25 (30 µg/mouse) on day 17 and day 20 after tumor inoculation. Tumor volumes over time are depicted. (H and I) Kaplan-Meier survival analyses were performed based on the data in (F) and (G). The statistical significance of the difference between Ipi25 and Ipi13 with Ipi was determined using the log-rank test. Data are presented as the mean  $\pm$  SEM. \*P < 0.05, \*\*P < 0.01, \*\*\*\*P < 0.001, and \*\*\*\*\*P < 0.0001. Representative data of two or three independent experiments are shown.

Ipi25 Shows Augmented Antitumor Efficacy. To evaluate antitumor efficacy, we compared Ipi13, Ipi25, and Ipi using the YUMM3.3 melanoma and MC38 colon tumor models. First, we inoculated Ctla4h/h mice subcutaneously with YUMM3.3 melanoma cells and then injected them with hIgG, Ipi, Ipi13, or Ipi25 antibodies (30 µg/dose/mouse) on days 10, 13, and 16.

Tumor size was then measured for up to 34 d in a masked fashion. While all ACAs significantly reduced tumor growth compared to the hIgG control group, Ipi25 caused a more pronounced effect than Ipi13 and Ipi, as exhibited by less melanoma growth in individual animals and increased number of tumor-free mice (Fig. 1*F* and *SI Appendix*, Fig. S3*C*).

Next, we tested the ACAs in the MC38 colon cancer model, by injecting MC38 colon cells subcutaneously followed by i.p. administration (30 µg/dose/mouse) of hIgG, Ipi, Ipi13, or Ipi25 on days 17 and 19 (Fig. 1G). At 38 d, all ACAs showed a significant suppression of tumor growth, but Ipi25 achieved a significantly better outcome than Ipi or Ipi13. Kaplan–Meier survival plots with 100 and 150 d follow-up for melanomas and colon cancer, respectively, (using a threshold of 2,000 mm³ as the survival endpoint based on early removal criteria in the protocol), showed that Ipi and both variants had a significant rescue effect, with Ipi25 showing significantly longer survival compared to the others (Fig. 1 H and I). Of note, Ipi13 and Ipi were generally comparable in antitumor activity.

EE Dissociation of ACA Prevents Lysosomal Targeting and Degradation of CTLA-4. Based on the in vivo biological effects observed, we sought to explain how pH 6.0 disassociation could improve the performance of an ACA. It is established that the internal vesicular pH range for the EE, LE, and the lysosome is pH 6.0 to 6.5; pH 5.0 to 5.8; and pH 4.5 to 5.0, respectively (31). We therefore hypothesized that the distinct pH sensitivity of Ipi25 and Ipi13 may cause them to dissociate from CTLA-4 in different compartments, the EE or LE, respectively. To test this hypothesis, we examined the intracellular trafficking of the CTLA-4:ACA complex after antibody treatment. The endocytic vesicles can be marked by staining for the Rab family of monomeric GTPases (SI Appendix, Fig. S4): Rab5 for EE, Rab7 for LE, and Rab11 for recycling endosome (RE) (32, 33). We examined the colocalization of CTLA-4 and AF647-conjugated ACAs with Rab5+ and Rab7+ organelles. To investigate the trafficking of CTLA-4:ACA to lysosomes, we employed lysosomal assays such as lysotracker in live cell experiments. To maintain continuity with our previous approach, we utilized fluorescently labeled Rab-fusion constructs to examine the endosomal trafficking of CTLA-4:ACA within live cells. Comparing Rab expression via Rab-staining and transfected DsRed-hRabs showed no significant differences in the localization pattern of Rabs and their colocalization with CTLA-4 (SI Appendix, Fig. S5), suggesting that the overexpression of Rabs did not interfere with endosomal trafficking. Therefore, the observed pattern of Rabs in our data accurately represents the endosomal trafficking of ACA or ACAbound CTLA-4 within cells, without any disruptions caused by the Rab-fusion constructs. Hela cells stably expressing human CTLA-4-GFP (Hela-4-GFP) were transfected with DsRed-hRab5 or DsRed-hRab7 plasmids and stained with AF647-conjugated ACAs at 4 °C. After the unbound antibody was washed away, cells were transferred to 37 °C for 1 h, and the localization of the endocytosed Ipi:CTLA-4 complexes were evaluated by confocal microscopy (Fig. 2). We found that all ACA:CTLA-4 complexes were internalized into intracellular vesicles after the temperature shift (Fig. 2A). Both Ipi and Ipi13 colocalized with CTLA-4, Rab5, Rab7, indicating that, following incubation at 37 °C, these ACA:CTLA-4 complexes transited intact into Rab5+ EE (Fig. 2 A and C, Left) and Rab7<sup>+</sup> LE (Fig. 2 B and C, Right). By contrast, we found that Ipi25 and CTLA-4 showed a strikingly different pattern of separation at 1 h after temperature shift. While either CTLA-4 or Ipi25 were cargos in Rab5+ EE, they were rarely found together in the Rab7<sup>+</sup> LE (Fig. 2 *A*–*C*), suggesting that they have separated in EE after endocytosis and are not targeted to the LE (Fig. 2B, red, blue, and green arrows).

To confirm the difference in CTLA-4 dissociation, we evaluated blots of cell lysates from HEK293T cells stably expressing human CTLA-4-OFP (293T-4-OFP) and treated with the ACAs followed by immunoprecipitation. The data showed that Ip13, Ipi25,

and Ipi all coprecipitated CTLA-4 equivalently after binding at 4 °C (Fig. 2 *D*, *Left* and *SI Appendix*, Fig. S6). However, after endocytosis was triggered by incubation at 37 °C, the Ipi25 variant coprecipitated significantly less CTLA-4 compared to either Ipi13 or Ipi (Fig. 2 *D*, *Right* and *SI Appendix*, Fig. S6), further confirming that CTLA-4 association with Ipi25 was selectively reduced. Since most of the CTLA-4 protein resides inside the cells, short-term incubation with ACA at 4 °C did not meaningfully alter total CTLA-4 protein, as expected (Fig. 2 *D*, *Lower*).

We examined the fate of the AF488-conjugated Ipi or Ipi13 complexes with CTLA-4 in CHO cells stably expressing human CTLA-4-OFP (CHO-4-OFP) after surface binding for 1 h at 4 °C and then endocytosis for 1 h at 37 °C. We found that the labeled Ipi and Ipi13 were internalized into intracellular puncta that largely overlapped with lysotracker, indicating they had trafficked to lysosomes (Fig. 2 E and F and SI Appendix, Fig. S7). By contrast, Ipi25 puncta were mostly distinct from CTLA-4 puncta or lysosomes after endocytosis (Fig. 2 E and F and SI Appendix, Fig. S7). We conclude that the rapid pH-sensitive dissociation of the Ipi25:CTLA-4 complexes in the EE avoided terminal deposition of the Ipi25 or CTLA-4 in lysosomes.

EE Dissociation Facilitates Recycling of CTLA-4 and Ipi25 to the Cell Surface. To analyze possible recycling of ACAs and CTLA-4 after their internalization, we used Rab11 as a RE marker in Hela-4-GFP cells. Cells stained for CTLA-4 and Rab11 without any ACA treatment showed numerous colocalization points of CTLA-4 and Rab11, indicating that a considerable amount of intracellular CTLA-4 enters the recycling (SI Appendix, Fig. S5). We allowed ACA to bind to CTLA-4 on the cell membrane at 4 °C and then internalize into cells at 37 °C. Thus, ACA bound only to cell surface CTLA-4, while a large fraction of intracellular CTLA-4 that colocalized with Rab11 for recycling remained unbound to ACA (Fig. 3A). We found that ACAs and especially CTLA-4 entered Rab11+ vesicles, although, surprisingly, they were not always in the same Rab11+ vesicle [Fig. 3 A-C, merge: CTLA-4 + Rab11: yellow; ACA and CTLA-4 (no Rab11): cyan and ACA + Rab11: pink]. Quantitation showed that the complex yielding Ipi25 and CTLA-4 produced the most overlap with Rab11 (Fig. 3 B and C and SI Appendix, Fig. S8), but they were not found in the same Rab11+ vesicles, implying that they dissociate in the EE and then sorted into distinct Rab11 REs for recycling. By contrast, both Ipi and Ipi13 remained associated with CTLA-4 and separate from Rab11<sup>+</sup> vesicles (Fig. 3 A and C, ACA + Rab11: cyan; SI Appendix, Fig. S8). Thus, Ipi and Ipi13, which cannot dissociate at the EE pH 6.0, apparently target CTLA-4 to the LE/lysosomal pathway, whereas Ipi25 and its associated CTLA-4 redistribute to the Rab11+ RE pathway. Consequently, unlike Ipi and Ipi13, nearly all of the CTLA-4 in cells treated with Ipi25 colocalize with Rab11+ RE, but not the antibody itself (Fig. 3 B and C).

Additionally, there is minimal colocalization of the ACA and Rab11 for parental Ipi and Ipi13, but much greater for Ipi25 (Fig. 3C), suggesting that Ipi25 is more likely to be recycled and released outside the cell for reuse. To test whether Ipi25 is recycled as functional antibodies, we incubated ACAs with either control CHO or CHO-4-OFP. After washing away unbound antibodies, the antibody-coated cells were incubated at 37 °C for 4 h before the supernatants were collected to measure anti-CTLA-4 antibodies. The data showed that Ipi25 had a higher rate of recycling and secretion into the supernatants of CTLA-4-expressing cells compared to both Ipi and Ipi13 (Fig. 3D).

To confirm the above observations in human lymphocytes, we tested CTLA-4<sup>hi</sup> T lymphocytes (Tregs) from activated peripheral

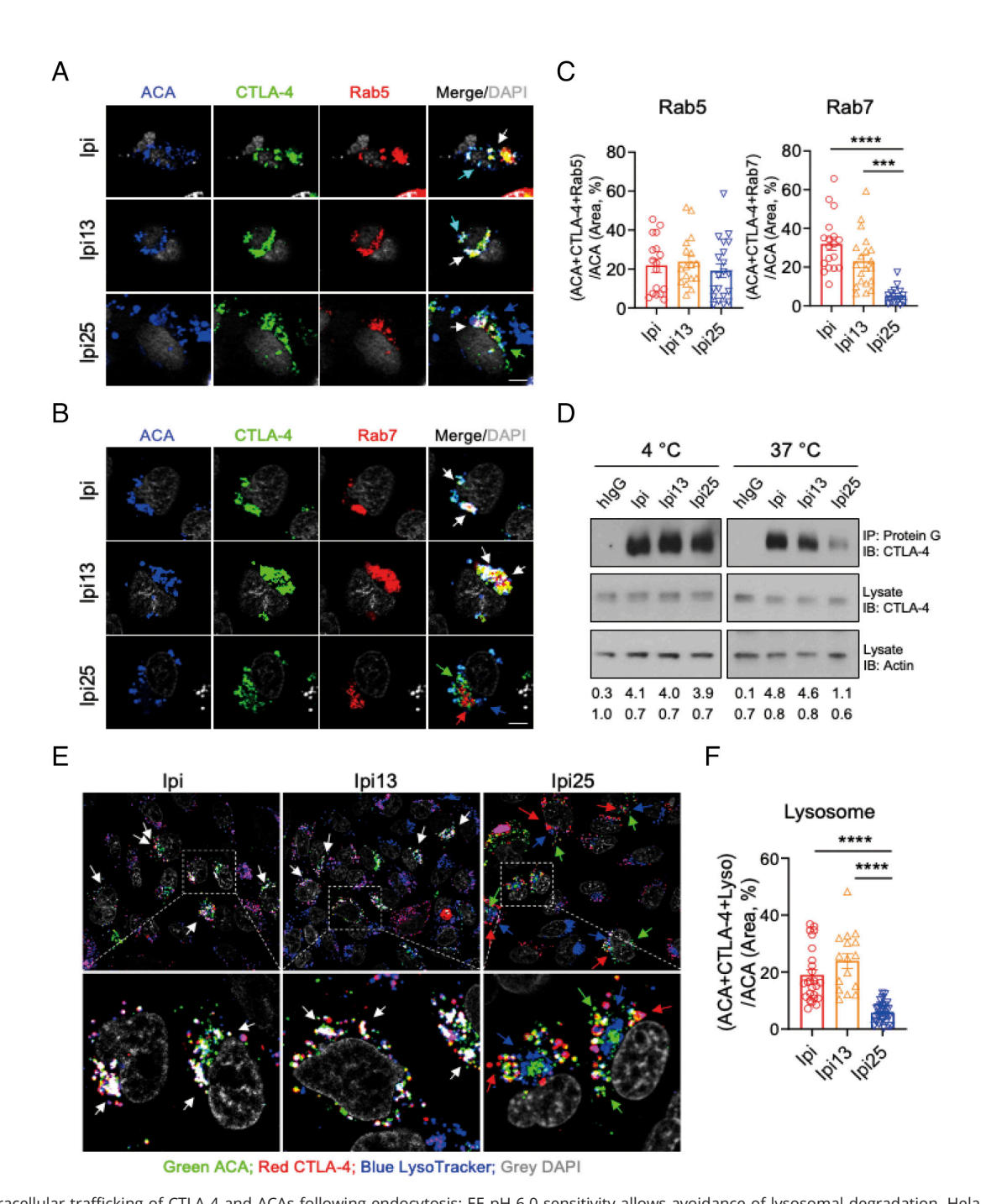


Fig. 2. Intracellular trafficking of CTLA-4 and ACAs following endocytosis: EE pH 6.0 sensitivity allows avoidance of lysosomal degradation. Hela-4-GFP were transfected with DsRed-hRab5 in (A) and DsRed-hRab7 in (B). The internalization of AF647-conjugated Ipi, Ipi13, or Ipi25 and Rabs is shown (ACA, blue; CTLA-4, green; Rab5/7, red; DAPI, light gray; merge of all three markers, white). Representative images from two to three independent experiments are displayed, with arrows indicating areas of colocalization. (Scale bar, 5 µM.) (C) The quantitation of the colocalized ACA, CTLA-4, and Rab within total ACA in (A) and (B) has been shown (n  $\approx$  20 cells/group). (D) 293 T-4-OFP were incubated with hlgG, lpi, lpi13, or lpi25 at 4 °C for 30 min. After washing off unbound antibody, the cells were either kept at 4 °C or transferred to 37 °C for 1 h. The antibody-bound surface CTLA-4 was immunoprecipitated (IP) using protein G beads and subsequently tested by immunoblot (IB). Representative images from two to three independent experiments are displayed. (E) Confocal micrographs of CHO-4-OFP stained with either Ipi-AF488 or Ipi variants-AF488 at 4 °C for 30 min and then washed and transferred to 37 °C for 60 min with lysotracker staining to visualize the colocalization between ACAs and lysosomes. (ACA, green; CTLA-4; red; lysosomes, blue; DAPI, light gray; merge of all three markers, write). Representative images from two to three independent experiments are displayed, with arrows indicating colocalization. (Scale bar, 5 µM.) (F) The quantitation of the colocalized ACA, CTLA-4, and lysotracker within total ACA in (E) has been shown (n  $\approx$  20 cells/group). Data were analyzed by a one-way ANOVA with Bonferroni's multiple comparison test. \*\*\*P < 0.001 and \*\*\*\*P < 0.0001. Representative data of three independent experiments are shown.

blood mononuclear cells (PBMCs) from healthy human donors. Using confocal microscopy, we observed that at 37 °C, Ipi, Ipi13, and Ipi25 were all internalized into Rab5+ EE within 30 min but exited these vesicles completely by 60 min (Fig. 3 E, Left). Rab7+ LE staining showed a different pattern, in which both Ipi and Ipi13 exhibited significant colocalization at 30 min that persisted at 60 min, but Ipi25 showed essentially no colocalization at either

time point (Fig. 3 E, Middle). Rab11+ vesicles were found to contain Ipi25, but not Ipi or Ipi13 (Fig. 3 E, Right). The quantitation of these results at 30 and 60 min verified that, at 60 min, Ipi and Ipi13 continued to accumulate in Rab7+ LE, but Ipi25 significantly diverged from the EE/LE pathway and accumulated in Rab11<sup>+</sup> RE (Fig. 3 *E* and *F*). Thus, the unique trafficking patterns for the Ipi variants were recapitulated in human Tregs.

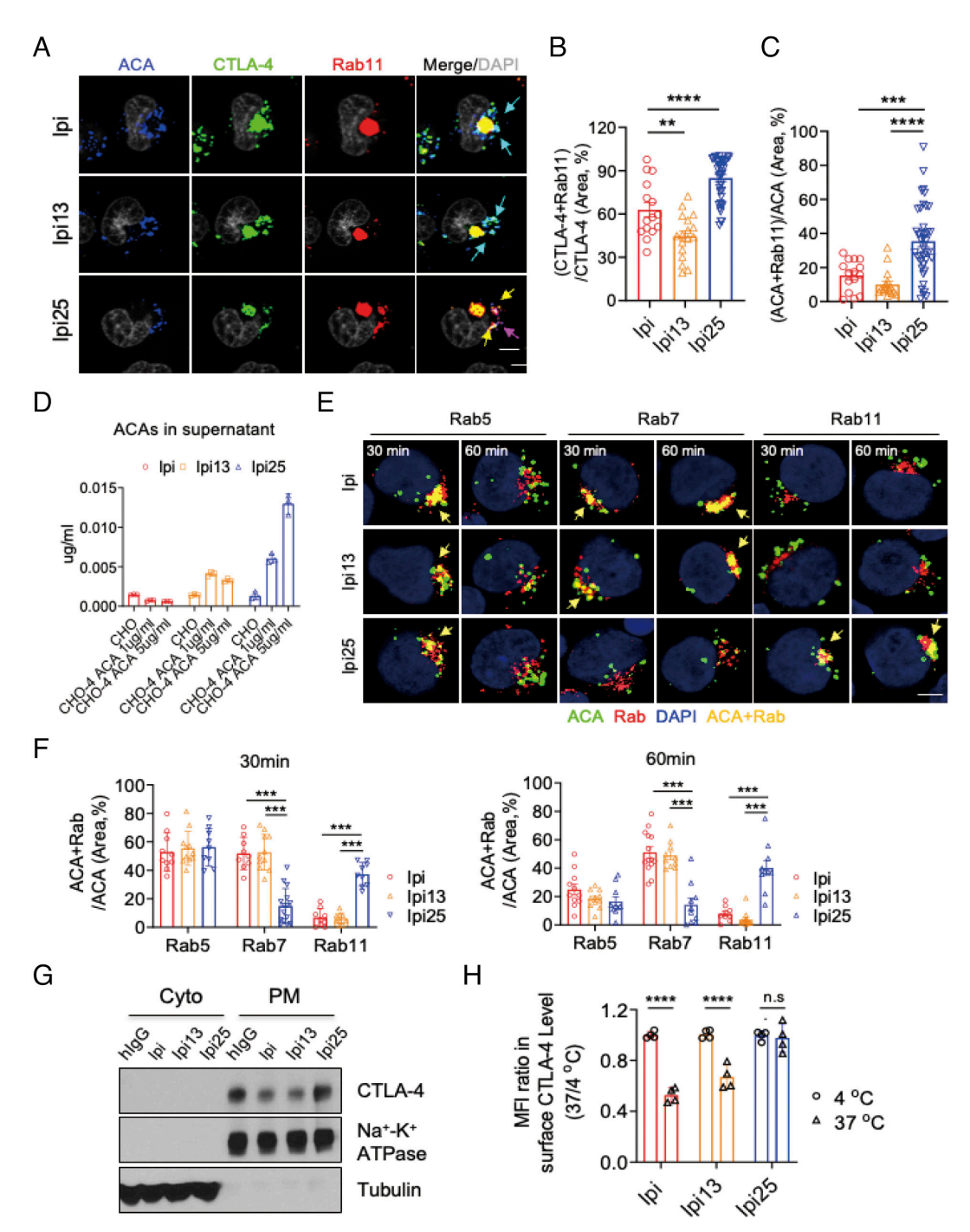


Fig. 3. EE pH 6.0-sensitive Ipi variants allow CTLA-4 and ACAs to enter RE. (A) Confocal microscopy of Hela-4-GFP transfected with DsRed-hRab11. The internalization of AF647-conjugated Ipi, Ipi13, or Ipi25 and Rab11 is shown (ACA, blue; CTLA-4, green; Rab11, red; DAPI, light gray; CTLA-4 + ACA, cyan; CTLA-4+ Rab11 yellow; ACA + Rab11, magenta). Representative images from two to three independent experiments are displayed, with arrows indicating colocalization. (Scale bar, 5 µM.) (B) The quantitation of the colocalized ACA and Rab11 within total ACA in (A) has been shown (n = 20 to 40 cells/group). (C) The quantitation of the colocalized CTLA-4 and Rab11 within total ACA in (A) has been shown (n = 20 to 40 cells/group). (D) CHO or CHO-4-OFP were treated with Ipi, Ipi13, or Ipi25 (1 µg/mL or 5 µg/mL) at 4 °C for 30 min. After washing out unbound antibody, the cells were incubated at 37 °C for 4 h. Culture medium of treated cells was collected, and the concentration of released ACAs was measured by ELISA. (E) Activated human lymphocytes were incubated at 4 °C for 30 min and then stained with AF647-conjugated Ipi, Ipi13, or Ipi25 at 4 °C for 1 h, followed by a switch to 37 °C for 30 min or 60 min after washing away unbound antibody. Cells were stained with anti-Rab5, Rab7, or Rab11, as indicated, along with DAPI. Confocal microscopy was used to capture images. Representative images from three independent experiments are displayed, with arrows indicating areas of colocalization (ACA, green; Rabs, red; nuclei, blue; yellow: ACA + Rabs). (Scale bar, 5 µM.) (F) The colocalization between ACA and Rabs was analyzed with ImageJ software to quantify fluorescent area, and the results are shown as the percentage of ACA and Rabs colocated area in ACA area (n = 9 to 15 cells/group). (ACA, green; Rabs, red; nuclei are shown as blue; ACA + Rabs, yellow). Results are representative of three independent experiments, and each image was chosen randomly. (G) Immunoblots of 293T-4-OFP incubated with control hlgG, Ipi, Ipi13, or Ipi25 for 4 h. Western blots of proteins from isolated cytosolic (Cyto) and PM fractions probed for the indicated proteins. (H) Mean fluorescence intensity (MFI) ratios from flow cytometry analysis of CTLA-4 surface level on CHO-4-OFP cells stained with hlgG, lpi, lpi13, or lpi25 without  $(4 \, ^{\circ}\text{C})$  or with  $(37 \, ^{\circ}\text{C})$  endocytosis. MFI at  $37 \, ^{\circ}\text{C}$  was divided by MFI at  $4 \, ^{\circ}\text{C}$  (defined as 1) to give the MFI ratio. Experiments in this figure have been repeated for three times. Data were analyzed by one-way ANOVA with Bonferroni's multiple comparison test. \*\*P < 0.001, and \*\*\*\*P < 0.0001. Representative data of three independent experiments are shown.

To clarify the final destination of CTLA-4, we isolated cytoplasmic vs. plasma membrane (PM) fractions in human 293 T-4-OFP cells, marked by tubulin or Na+-K+ ATPase, respectively, at 4 h postexposure to the ACAs at 37 °C. We found that Ipi and Ipi13 significantly reduced CTLA-4 in the PM and no CTLA-4 was detected in the cytosol (supernatant) under any condition (Fig. 3G and SI Appendix, Fig. S9). By contrast, Ipi25 and the hIgG control did not reduce cell surface CTLA-4 (Fig. 3G and SI Appendix, Fig. S9). To corroborate this observation, we compared ACA down-modulatory effects on CTLA-4 by flow cytometry. CTLA-4-expressing cells were treated with Ipi, Ipi13, or Ipi25 either at 4 °C or 37 °C and cell surface antibody-bound CTLA-4 was measured using an AF488-conjugated anti-human IgG Fc secondary antibody. We observed that Ipi and Ipi13 markedly reduced surface CTLA-4, but it was preserved with Ipi25, indicating that this antibody causes a downregulation and recovery of CTLA-4 presumably by releasing it to recycle to the cell surface (Fig. 3H and SI Appendix, Fig. S10).

EE pH 6.0 Sensitivity but Not General Low Affinity of Target Binding Determines the Safety and Efficacy of Anti-CTLA-4 Antibodies. Given the unique trafficking and improved clinical properties of Ipi25, we also questioned whether its generally lower affinity to CTLA-4 (SI Appendix, Fig. S2A, fourfold increased K<sub>D</sub>), rather than selective dissociation at EE pH 6.0, explained its properties. Therefore, we evaluated another Ipi variant, Ipi14 for pH sensitivity, irAEs, and antitumor activity. Ipi14 and Ipi25 had similar binding to CTLA-4 at neutral pH, but Ipi14 largely maintained high binding at pH 6.0, similar to Ipi and Ipi13 (SI Appendix, Figs. S11 A and B and S12). First, to determine whether it allows recycling, we examined surface CTLA-4 and found that like Ipi and Ipi13, Ipi14 significantly reducing surface CTLA-4 levels, presumably through lysosomal degradation, whereas Ipi25 preserved CTLA-4 as previously observed (SI Appendix, Fig. S11 C and D). We also observed significant irAEs after injecting Ipi14 including worse growth retardation compared to the Ipi (SI Appendix, Fig. S11E) as well as declines in total hemoglobin (Hb) and hematocrit (HCT) levels (SI Appendix, Fig. S11F). In addition, we compared the antitumor efficacy of Ipi14 and Ipi in the MC38 colon tumor model and found that although both antibodies significantly suppressed tumor growth compared with hIgG controls, Ipi14 had significantly worse antitumor efficacy than Ipi (SI Appendix, Fig. S11 G and H). Together, these data indicate that Ipi14, while sharing low affinity of Ipi25, fails to specifically dissociate at pH 6.0 and shares none of the beneficial properties of Ipi25 including preservation of surface CTLA-4, the lack of significant irAEs, and better tumor efficacy. Thus, reduced affinity overall at neutral pH is not itself a beneficial property. The conventional wisdom for developing ACA up until now is that ACA with high affinity is believed to exert their antitumor efficacy by interfering with receptor-costimulatory ligand interactions. Consequently, numerous ACAs with robust binding capabilities, such as Ipi and Treme, have been developed for clinical use (34–36). However, our study reveals that optimal therapeutic outcomes do not solely depend on high-affinity binding. ACA with weak affinity but pH 6.0 sensitivity is critical for enhancing ACA's therapeutic index. These findings underscore the importance of considering diverse factors in ACA design strategies.

## Engineered Variants for EE pH 6.0 Dissociation of Tremelimumab. To generalize the principle of engineering ACA for EE pH 6.0sensitive dissociation to improve ACAs, we generated a panel of Tyr to His variants in Treme, the other major ACA in current clinical use (37, 38). To facilitate mouse experiments, we constructed TremeIgG1,

a chimeric IgG1 variant of Treme containing the human IgG1

constant region, which is needed for therapeutic activity in mice, and the variable regions of Treme. We selected 4 pH-sensitive variants Treme156-159 and evaluated the pH sensitivity of their binding under EE (pH 6.0 to 6.5), LE (pH 5.0 to 5.5), and lysosome (pH 4.5 to 5.0) conditions. The binding of TremeIgG1 to CTLA-4 was insensitive to pH between pH 4.0 and pH 7.0, whereas the four variants showed different patterns. Treme156 and Treme157 showed dissociation starting at pH 6.0; while Treme158 and Treme159 dissociated only at pH 5.5 or lower (SI Appendix, Fig. S13). Based on previously reported data, all five Treme variants have strong binding at pH 7.4 with low to subnanomolar affinity (28). However, when we performed SPR analysis at pH 6.0, these variants fell into two groups, the group 1 variants (Treme156, 157) had lower CTLA-4 affinity (KD = 8.93  $\times$  10<sup>-8</sup> M for Treme156 and 1.04  $\times$  10<sup>-7</sup> M for Treme157) at pH 6.0 and can be considered EE pH 6.0 sensitive and the group two variants (TremeIgG1, Treme158, and Treme159) were considered EE pH 6.0 insensitive as they retained nanomolar affinity at pH 6.0 (Fig. 4A). We then measured the dissociation of ACA by binding the variants to CTLA-4 at neutral pH and subsequently washing the preformed complexes with buffer at different acidic pHs (Fig. 4 B, Left). When normalized to binding at pH 7.0, TremeIgG1, Treme158, and Treme 159 maintained high binding at pH 6.0. By contrast, Treme 156 and Treme 157 significantly dissociated from CTLA-4 at pH equivalent to or below EE pH 6.0 (Fig. 4 B, Right). Thus, the two groups of Treme variants showed distinct dissociation at pH 6.0.

Using the anti-PD-1 irAE model described in Fig. 1, we found that mice treated with the Treme EE pH 6.0-stable variants, Treme158 and Treme159, exhibited significant growth retardation beginning at 12 d, whereas only slight growth retardation was observed in mice receiving the EE pH 6.0-sensitive Treme156 and Treme157 compared to the hIgG control (Fig. 4 C and D and SI Appendix, Fig. S14). Importantly, the EE pH 6.0-insensitive variants caused progressive mortality up to 90% starting on day 19 (Fig. 4E). The mortality was reduced to 20% in mice treated with the EE pH 6.0-sensitive Treme 156 or 157 (Fig. 4E). These findings demonstrated that dissociation at EE pH 6.0, is associated with dramatically improved safety.

To test antitumor activity, we compared the efficacy of Treme variants in retarding MC38 tumor growth. We administered 3 doses of 0.5 mg/kg/dose of antibodies on day 7, day 10, and day 13 after tumor inoculation when tumors were approximately 5 to 6 mm in diameter, or 1.5 mg/kg/dose of antibodies on day 17 and day 20 after tumor inoculation when tumors had grown to an average size of 10 mm in diameter. At these restricted doses, all ACAs led to significant tumor rejection, but the EE pH 6.0sensitive variant group exhibited enhanced efficacy compared to the EE pH 6.0-insensitive variant group (Fig. 4F). Taken together, our data indicate that transforming a pH 6.0-insensitive ACA into an EE pH 6.0-sensitive ACA also improved another clinically important immunotherapeutic ACA.

EE pH 6.0 Sensitivity Enhances the Depletion of Intratumoral Tregs by Avoiding ACA-Induced CTLA-4 Downregulation. Previous studies have demonstrated that ACAs selectively deplete tumor Treg through ADCC and/or ADCP (23-25, 28). This is thought to be one of the primary mechanisms for ACA's antitumor activity (23-25, 28). Our previous study established that by preventing antibody-induced CTLA-4 degradation, ACA that are pH sensitive have better ADCC activity and higher efficacy in Treg depletion in the tumor microenvironment. We therefore explored whether the improved therapeutic activity of the EE pH 6.0-sensitive Ipi and Treme variants is attributable to better Treg depletion. To do so, we measured the surface CTLA-4 on tumor-infiltrating Tregs and antibody-induced Treg depletion

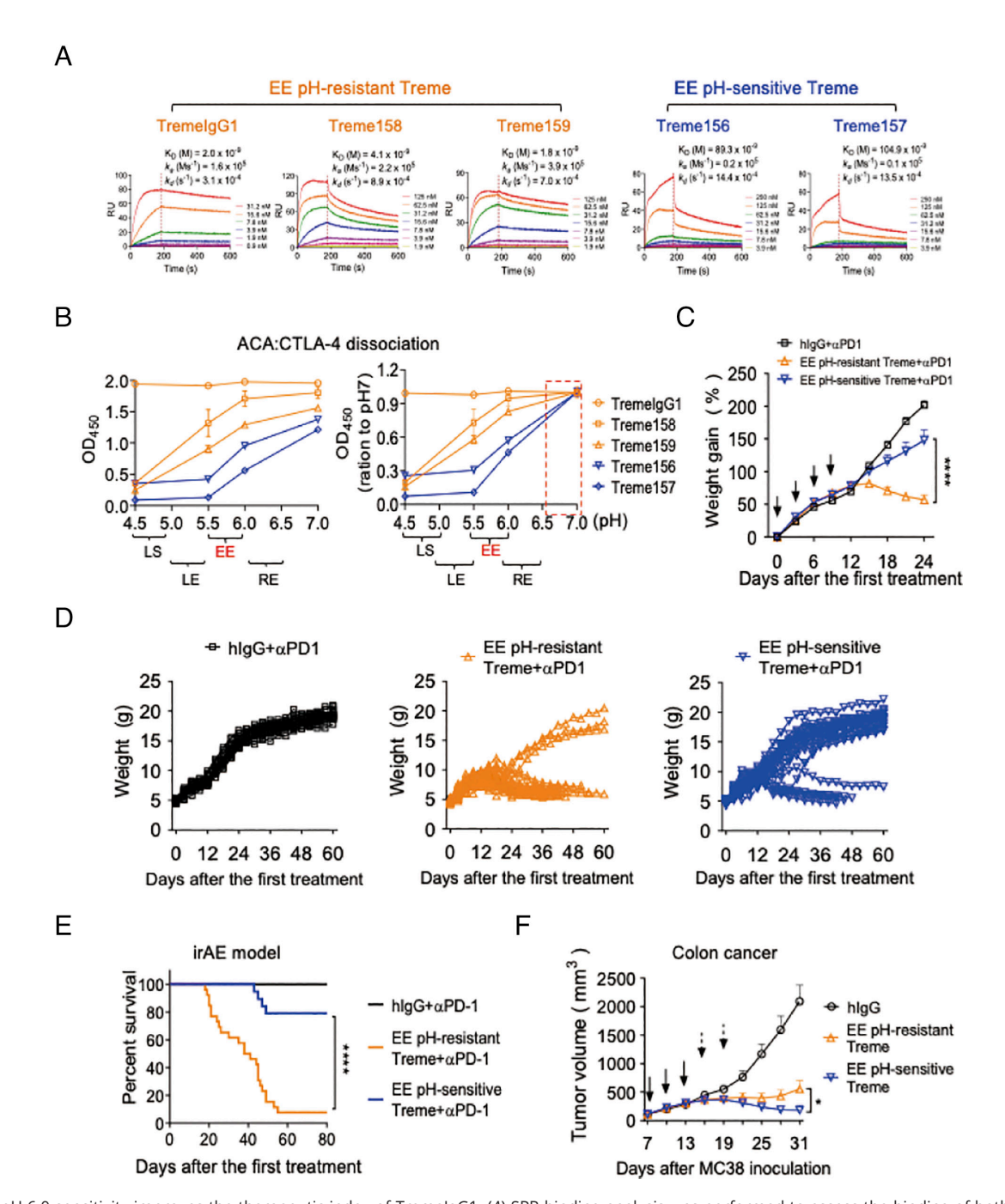


**Fig. 4.** EE pH 6.0 sensitivity improves the therapeutic index of TremelgG1. (*A*) SPR binding analysis was performed to assess the binding of both EE pH 6.0-insensitive Treme variants and the EE pH 6.0-sensitive Treme variants to his-hCTLA-4 at pH 6.0. A twofold titration series of his-CTLA-4 was used for each variant (pH 6.0: 0.9 to 31.2 nM for TremelgG1; 1.9 to 125 nM for Treme158 and Treme159; 3.9 to 250 nM for Treme156 and Treme157). (*B*) The pH-sensitive dissociation of the Treme variants was examined and shown as the means of duplicate optical density at 450 nm (*Left*) and showed as a ratio with the value at pH 7 (*Right*). (*C*) Ten-day-old C57BL/6 Ctla4<sup>h/h</sup> mice [body weight: 4.5 to 5.3 g) were treated with different regimens: control hlgG plus αPD-1 (n = 15), the EE pH 6.0-insensitive Treme (TremelgG1: n = 14, Treme158: n = 5 and Treme159: n = 6) plus αPD-1 (n = 25 in total), or the EE pH 6.0-sensitive Treme (Treme156: n = 6 and Treme157: n = 14) plus αPD-1 (n = 20 in total). The treatment was administered at a dose of 100 μg/mouse/injection on days 10, 13, 16, and 19 after birth. The body weight over time is presented as the mean percentage weight gain following the first injection with SEM. (*D*) The body weight of each mouse in (*C*) is displayed for reference. (*E*) Kaplan-Meier survival analysis was conducted based on the data in (*C* and *D*). The statistical significance of the difference between the EE pH 6.0-insensitive plus αPD-1 group or EE pH 6.0-sensitive plus αPD-1 group was determined using the log-rank test. (*F*) MC38 tumor-bearing Ctla4<sup>h/h</sup> mice were injected i.p. with three doses of 0.5 mg/kg/dose of antibodies (hlgG: n = 5; EE pH 6.0-insensitive TremelgG1: n = 15; EE pH 6.0-sensitive TremelgG1: n = 10) on day 7, day 10, and day 13 after tumor inoculation (when tumors were around 5 to 6 mm in diameter, representing small tumors), or 1.5 mg/kg/dose of antibodies (hlgG: n = 12; EE pH 6.0-insensitive TremelgG1: n = 17; EE pH 6.0-sensitive TremelgG1: n = 12) on day 17 and day 20 a

in an ACA-treated melanoma model. The gating strategy for intratumor Tregs has been shown in *SI Appendix*, Fig. S15. We found that whereas both Ipi13 and Ipi potently decreased cell surface CTLA-4 levels on tumor-infiltrating Tregs, Ipi25 caused

only slight CTLA-4 downregulation compared to the hIgG control (Fig. 5 *A* and *B*). No differences in the lower level of CTLA-4 expressed on splenocytes were observed between variants (Fig. 5*B*). More importantly, while Ipi13 and Ipi treatment caused

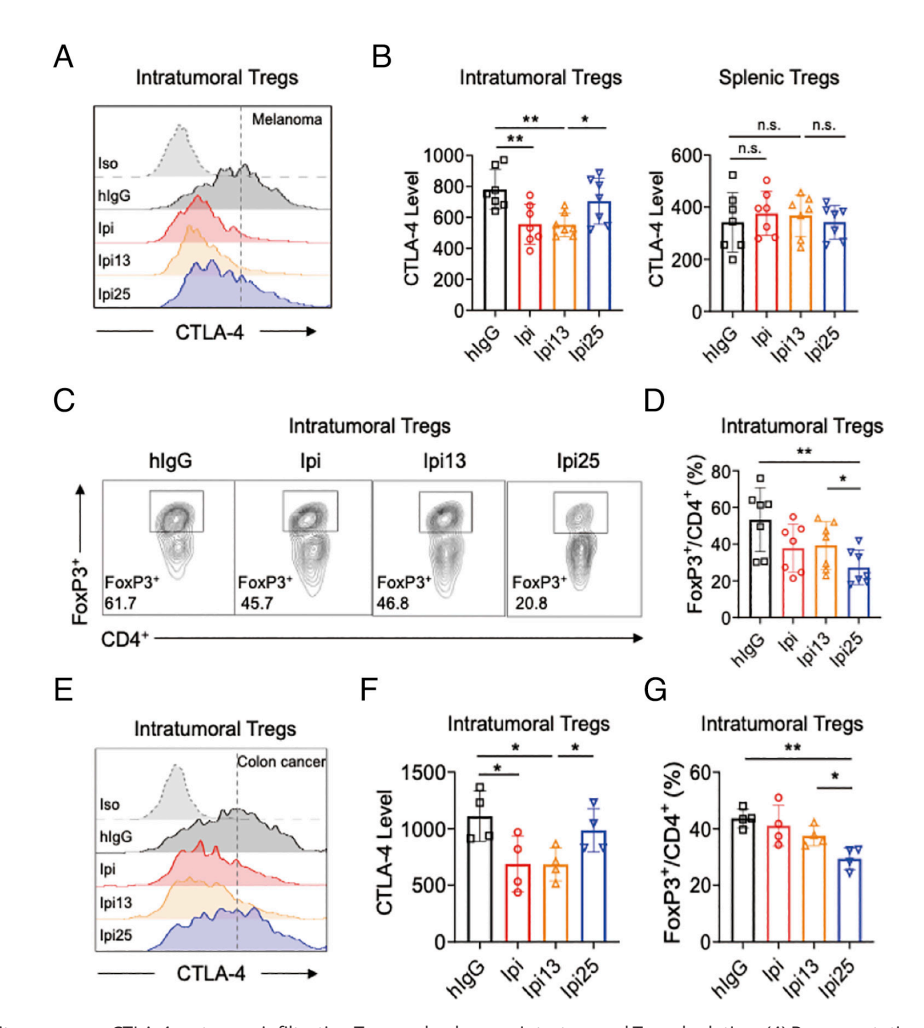


Fig. 5. EE pH 6.0 sensitivity preserves CTLA-4 on tumor-infiltrating Treg and enhances intratumoral Treg depletion. (A) Representative flow cytometry histograms of CTLA-4 on YUMM3.3 tumors from Ctla4<sup>h/h</sup> mice (n = 7) treated with Ipi, Ipi13, or Ipi25 (100 μg/mouse) on day 14 after tumor inoculation. Surface CTLA-4 of tumor-infiltrating Tregs was measured by flow cytometry in the presence of excess antibodies to avoid antibody masking. Representative histograms of flow cytometry of cell surface CTLA-4 staining on tumor Tregs have been shown. (B) MFI of cell surface CTLA-4 level on tumor Treg (Left) and spleen Treg (Right) in (A) have been shown. (C and D) Measurement of Treg in (A and B) as a fraction of CD4+ cells isolated from tumor tissue was assessed by intracellular FoxP3 staining at 24 h after antibody treatment. Representative flow cytometry data (C) and the corresponding quantification (D) are provided. Experiments in (A–D) have been repeated two times, and the data were combined as two independent experiments. (E) MC38-bearing Ctla4 $^{h/h}$  mice (n = 4) were treated with Ipi, Ipi13, or Ipi25 (100 μg/mouse) on day 14 after tumor inoculation. Surface CTLA-4 of tumor-infiltrating Tregs was measured by flow cytometry in the presence of excess antibodies to avoid the influence of antibody masking. Representative histograms of flow cytometry of cell surface CTLA-4 staining on tumor Tregs have been shown. (F) MFI of cell surface CTLA-4 level on tumor Treg in (E) has been shown. (G) Measurement of tumor Treg in (E and F) by intracellular FoxP3 staining at 24 h after antibody treatment was provided. Data were analyzed by one-way ANOVA with Bonferroni's multiple comparison test. \*P < 0.05 and \*\*P < 0.01. Representative data of three independent experiments are shown.

only modest reduction in tumor-infiltrating CD4+ FoxP3+, we observed much better Treg depletion by Ipi25 treatment (Fig. 5 C and D). The frequency of tumor-infiltrating Tregs in the Ipi25treated tumors was significantly lower than those found in the Ipi13-treated tumors (Fig. 5 C and D). Regardless of the ACA used, Treg-depletion occurs specifically within tumors, but not in the spleen (SI Appendix, Fig. S16). We and others have attributed the lack of splenic Treg depletion to lower CTLA-4 expression (22, 25, 28).

To validate these findings, we repeated these analyses in the MC38 colon cancer model. This yielded comparable results. Ipi13 and Ipi reduced CTLA-4 levels on tumor Tregs, but Ipi25 maintained cell surface CTLA-4 on tumor Tregs, almost to the level of the IgG control group (Fig. 5 E and F). Additionally, Ipi25 facilitated Treg depletion within the tumors more effectively than Ipi13 or Ipi (Fig. 5G). As expected, no significant decrease in CD4+ FoxP3+ Tregs were observed in the spleen across all ACA-treated groups (SI Appendix, Fig. S17). Furthermore, there was no observable impact of the ACAs on tumor-infiltrating CD4<sup>+</sup> and CD8<sup>+</sup> T cells (SI Appendix, Fig. S18).

#### **Discussion**

Severe irAE have prevented currently approved ACA to be dosed in a manner to reach their full therapeutic potential, as suggested by the fundamental biology of CTLA-4 in tumor evasion of host immunity (19, 38). Here, we undertook a systematic approach to generate variants of clinically approved ACAs to achieve fewer irAE and greater therapeutic effectiveness. We modified two ACAapproved drugs, Ipi and Treme, to explore whether enhancing the pH sensitivity of binding to CTLA-4 would improve their therapeutic indices. By substituting Tyr with His in the CDRs of Ipi, we successfully generated a library of pH-sensitive Ipi variants. Surprisingly, not all variants that were acidic pH-sensitive exhibited a reduction in irAE or improved antitumor activity as we had previously conjectured (28). Our analyses of variants for Ipi and Treme suggest that ACAs need to significantly dissociate from CTLA-4 at pH 6.0 to meaningfully improve therapeutic effects and reduce irAEs. Also, the loss of cell surface CTLA-4 caused by ACAs, which may previously have been thought to be beneficial (1 to 3), is correlated in our experiments with worse antitumor efficacy and worse irAEs and ameliorated by ACAs that maintain high CTLA-4 cell surface expression.

Mechanistically, all ACAs bind cell surface CTLA-4 and trigger antibody-induced endocytosis, but the fate of the ACA and CTLA-4 are finely tuned by the specific pH at which the ACA and CTLA-4 dissociate. The EE pH 6.0-insensitive variants (dissociating at pH 5.5 or less or not dissociating at all) remain bound to CTLA-4 in the EE and convey CTLA-4 into LE/lysosome for degradation, as we have described for the parental Mabs Ipi and tremeIgG1 (28). By contrast, the EE pH 6.0-sensitive variants dissociate from CTLA-4 in the EE and allow CTLA-4 to be transported to RE for recycling (SI Appendix, Fig. S19). Interestingly, both released CTLA-4 and ACA were recycled but not always found in the same Rab11 vesicles (Fig. 3A), implying that they dissociate in the EE and then sorted into distinct Rab11 REs for recycling using different recycling mechanisms. CTLA-4 recycling relies on its interaction with LRBA, which safeguards CTLA-4 from lysosomal degradation and facilitates recycling back to the cell surface (13-15). Our prior investigation revealed that postendocytosis, Ipi remains bound to CTLA-4, hindering its recycling (28). EE pH 6.0-sensitive variant Ipi25 dissociates from CTLA-4 within the EE allowing it to undergo recycling. Recycling of endocytosed antibodies recycle typically occurs via the neonatal Fc receptor (FcRn) (39). However, since Tregs do not express FcRn, further studies are needed to understand the mechanisms underlying ACA recycling.

Preserving CTLA-4 recycling appears to confer a dual advantage for EE pH 6.0 sensitive ACA. Recycling is critical in protecting the host against autoimmune diseases (28). We now show that ACA that dissociate in the EE allow greater CTLA-4 recycling leading to a dramatically reduced irAE profile. Additionally, recycling preserves cell surface CTLA-4 on tumor Tregs as a target for ADCC/ADCP activity. The EE pH 6.0-sensitive variants enhance CTLA-4 selective Treg depletion in the TME and manifest increased tumor elimination. The recycling of EE pH 6.0-sensitive ACA itself should also increase local ACA concentration which could also contribute to the antitumor activity. While the benefits of preserving CTLA-4 have been confirmed experimentally (28), those conferred by ACA recycling remain to be further confirmed in vivo.

Another aspect to consider is how much the classic checkpoint inhibition of B7-1 and B7-2 would be affected by pH-sensitive dissociation. CTLA-4 recycling rather than degradation could facilitate its engagement of B7-1 and B7-2 on antigen-presenting cells as well as cause binding and removal of additional ACA. The latter effect may decrease the efficacy of checkpoint therapy. Moreover, preserving CTLA-4 in the TME may allow it to suppress antitumor immunity by reducing costimulatory molecules on antigen-presenting cells, thereby reducing the overall effectiveness of ACA. Since Ipi induced tumor rejection in heterozygous human/mouse CTLA-4 animals where it cannot fully block all B7-CTLA-4 interactions, checkpoint blockade may not be the sole mechanism for its antitumor efficacy (20). Due to the high levels of CTLA-4 constitutively expressed on the surface of tumor-infiltrating Treg, FcyR-dependent Treg depletion is selective for tumor-infiltrating Treg. Once Treg cells are depleted, their cell surface CTLA-4 would not play a role as sink of costimulatory molecules. It is likely that the dosing regimen of the modified ACAs that we have designed will determine antitumor effectiveness considering multiple countervailing mechanisms.

Antibody-induced endocytosis occurs often in immunotherapy and other cell surface immune checkpoint molecules also undergo internalization, recycling, and degradation (40-43). Our study suggests fine-tuning pH sensitivity to alter the intracellular trafficking and dissociation of both targets and antibodies as a valuable

avenue to engineer better therapeutic antibodies. This approach of endocytic recycling manipulation could be more generally applicable, but this will depend on the regulatory mechanisms of different targets. For instance, PD-1 and TIM-3 predominantly affect CD8<sup>+</sup>T cells within tumors. High levels of chec (40) kpoint binding can trigger ADCC and ADCP, resulting in the depletion of antitumor CD8+ T cells. Therefore, maintaining these immune checkpoint molecules with pH-sensitive antibodies may not be an effective treatment strategy compared to CTLA-4.

Taken together, our work reveals how EE pH 6.0 sensitivity affects the intracellular trafficking ACA and CTLA-4 and the therapeutic indices of ACA. This insight provides an approach to generate safer and more effective ACA. Transforming a pH-insensitive ACA into an EE pH 6.0-sensitive ACA may represent a potentially universal principle for engineering safer and more effective ACA therapy.

### **Materials and Methods**

Antibodies, reagents, animals, and detailed methods for all experiments can be found in SI Appendix, Materials and Methods. All animal experiments were approved by the Institutional Animal Care and Use Committee of Shanghai Jiao Tong University School of Medicine (Protocol approval number: JUMC2023-053-A) or the Institute of Human Virology at the University of Maryland Baltimore School of Medicine. Human whole blood was collected from healthy volunteers consented on protocols for human specimen collection under an approved clinical protocol (Ruijin Hospital Clinical Trail Ethics Committee approval number #2015-6).

Data, Materials, and Software Availability. All study data are included in the article and/or SI Appendix.

ACKNOWLEDGMENTS. We thank Dr. Zheng-gang Liu from National Cancer Institute for comments and suggestions. Part of the study was performed when some authors were at the Institute of Human Virology and Department of Surgery, University of Maryland School of Medicine, Baltimore. This work was supported by the Research Funding from the National Natural Science Foundation of China to Y.Z. (No. 82071866, No.82271762, and No. 82241227), Natural Science Foundation of Shanghai (22ZR1454800), National key research and development project of Ministry of Science and Technology (2023YFC2411403), Nanjing AcroImmune BioTech. Co., Ltd. (2023310031000221), and by the Division of Intramural Research of National Institute of Allergy and Infectious Diseases, NIH. Additionally, we would like to express our gratitude to Dr. Lieping Chen from Yale for his insightful comments, which have significantly enhanced our manuscript. Research grant from OncoC4, Inc.

Author affiliations: <sup>a</sup>Department of Immunology and Microbiology, Shanghai Institute of Immunology, Shanghai Jiao Tong University School of Medicine, Shanghai 200025, China; Division of Immunotherapy, Institute of Human Virology, University of Maryland School of Medicine, Baltimore, MD 21201; 'Key Laboratory of Infection and Immunity of Shandong Province and Department of Immunology, School of Basic Medical Sciences, Shandong University, Jinan 250012, China; <sup>d</sup>State Key Laboratory of Biotherapy, West China Hospital, Sichuan University, Chengdu 610041, Sichuan, China; <sup>e</sup>Beijing Pediatric Research Institute, Beijing Children's Hospital, National Center for Children's Health, Capital Medical University, Beijing 100045, China; 'Department of Biophysics and Biophysical Chemistry, Johns Hopkins School of Medicine, Baltimore, MD 21205; <sup>®</sup>Department of Endocrine and Metabolic Diseases, Shanghai Institute of Endocrine and Metabolic Diseases, Ruijin Hospital, Shanghai Jiao Tong University School of Medicine, Shanghai 200025, China; <sup>h</sup>Shanghai National Clinical Research Center for Metabolic Diseases, Key Laboratory for Endocrine and Metabolic Diseases of the National Health Commission of the People's Republic of China, Shanghai Key Laboratory for Endocrine Tumor, Ruijin Hospital, Shanghai Jiao Tong University School of Medicine, Shanghai 200025, China; 'OncoC4, Inc., Rockville, MD 20854; <sup>J</sup>Molecular Development of the Immune System Section, Laboratory of Immune System Biology, and Clinical Genomics Program, National Institute of Allergy and Infectious Diseases, NIH, Bethesda, MD 20814; and <sup>k</sup>Center for Immunerelated Diseases at Shanghai Institute of Immunology, Ruijin Hospital, Shanghai Jiao Tong University School of Medicine, Shanghai 200025, China

Author contributions: M.Z., J.L., P. Zhang, J.K.F., P. Zheng, Y.L., M.J.L., and Y.Z. designed research; M.Z., J.L., K.Y., H.Z., S.M., B.W., D.L., X.D., M.L., P. Zhang, J.K.F., L.Y., and Y.Z. performed research; Y.Z. contributed new reagents/analytic tools; M.Z., J.L., K.Y., S.M., X.D., P. Zhang, J.K.F., P. Zheng, Y.L., M.J.L., and Y.Z. analyzed data; and M.Z., S.M., P. Zheng, Y.L., M.J.L., and Y.Z. wrote the paper.

Reviewers: K.M.M., Washington University in St. Louis School of Medicine; and J.T., The University of North Carolina at Chapel Hill.

- M. A. Postow, R. Sidlow, M. D. Hellmann, Immune-related adverse events associated with immune checkpoint blockade. N. Engl. J. Med. 378, 158-168 (2018).
- A. Bertrand, M. Kostine, T. Barnetche, M. E. Truchetet, T. Schaeverbeke, Immune related adverse events associated with anti-CTLA-4 antibodies: Systematic review and meta-analysis. BMC Med. 13,
- G. Q. Phan et al., Cancer regression and autoimmunity induced by cytotoxic Tlymphocyte-associated antigen 4 blockade in patients with metastatic melanoma. Proc. Natl. Acad. Sci. U.S.A. 100, 8372-8377 (2003).
- K. E. Beck et al., Enterocolitis in patients with cancer after antibody blockade of cytotoxic T-
- lymphocyte-associated antigen 4. *J. Clin. Oncol.* **24**, 2283–2289 (2006).

  J. Weber, Review: Anti-CTLA-4 antibody ipilimumab: Case studies of clinical response and immunerelated adverse events. Oncologist 12, 864–872 (2007).
- P. Attia et al., Autoimmunity correlates with tumor regression in patients with metastatic melanoma treated with anti-cytotoxic T-lymphocyte antigen-4. J. Clin. Oncol. 23, 6043-6053 (2005).
- P. S. Linsley et al., CTLA-4 is a second receptor for the B cell activation antigen B7. J. Exp. Med. 174, 561-569 (1991).
- Y. Wu, Y. Guo, Y. Liu, A major costimulatory molecule on antigen-presenting cells, CTLA4 ligand A, is distinct from B7. J. Exp. Med. 178, 1789-1793 (1993).
- G. J. Freeman et al., Cloning of B7-2: A CTLA-4 counter-receptor that costimulates human T cell proliferation. Science 262, 909-911 (1993).
- E. A. Tivol et al., Loss of CTLA-4 leads to massive lymphoproliferation and fatal multiorgan tissue destruction, revealing a critical negative regulatory role of CTLA-4. Immunity 3, 541-547 (1995)
- P. Waterhouse et al., Lymphoproliferative disorders with early lethality in mice deficient in Ctla-4. 11 Science 270, 985-988 (1995).
- C. A. Chambers, T. J. Sullivan, J. P. Allison, Lymphoproliferation in CTLA-4-deficient mice is mediated by costimulation-dependent activation of CD4+T cells. *Immunity* **7**, 885–895 (1997). 12.
- B. Lo et al., Patients with LRBA deficiency show CTLA4 loss and immune dysregulation responsive to 13 abatacept therapy. Science 349, 436-440 (2015).
- $H.\,S.\,Kuehn\,\textit{et al.}, Immune\,dy sregulation\,in\,human\,subjects\,with\,heterozygous\,germline\,mutations$ 14. in CTLA4. Science 345, 1623-1627 (2014).
- T. Z. Hou et al., Identifying functional defects in patients with immune dysregulation due to LRBA and CTLA-4 mutations. Blood 129, 1458-1468 (2017).
- I. Bot, C. U. Blank, W. Boogerd, D. Brandsma, Neurological immune-related adverse events of ipilimumab. Pract. Neurol. 13, 278-280 (2013).
- F. Fadel, K. El Karoui, B. Knebelmann, Anti-CTLA4 antibody-induced lupus nephritis. N. Engl. J. Med. 361, 211-212 (2009).
- Y. Feng et al., Exposure-response relationships of the efficacy and safety of ipilimumab in patients with advanced melanoma. Clin. Cancer Res. 19, 3977-3986 (2013).
- Y. Liu, P. Zheng, Preserving the CTLA-4 checkpoint for safer and more effective cancer immunotherapy. Trends Pharmacol. Sci. 41, 4-12 (2020).
- X. Du et al., A reappraisal of CTLA-4 checkpoint blockade in cancer immunotherapy. Cell Res. 28, 20 416-432 (2018).
- X. Du et al., Uncoupling therapeutic from immunotherapy-related adverse effects for safer and effective anti-CTLA-4 antibodies in CTLA4 humanized mice. Cell Res. 28, 433-447 (2018).

- 22. M. J. Selby et al., Anti-CTLA-4 antibodies of IgG2a isotype enhance antitumor activity through reduction of intratumoral regulatory T cells. Cancer Immunol. Res. 1, 32-42 (2013).
- Y. Bulliard et al., Activating Fc gamma receptors contribute to the antitumor activities of immunoregulatory receptor-targeting antibodies. J. Exp. Med. 210, 1685-1693 (2013).
- T. R. Simpson et al., Fc-dependent depletion of tumor-infiltrating regulatory T cells co-defines the efficacy of anti-CTLA-4 therapy against melanoma. J. Exp. Med. 210, 1695-1710 (2013).
- F. Arce Vargas et al., Fc effector function contributes to the activity of human anti-CTLA-4 antibodies. Cancer Cell 33, 649-663.e4 (2018).
- E. Romano et al., Ipilimumab-dependent cell-mediated cytotoxicity of regulatory T cells ex vivo by nonclassical monocytes in melanoma patients. *Proc. Natl. Acad. Sci. U.S.A.* **112**, 6140-6145 (2015). 27. I. Yofe *et al.*, Anti-CTLA-4 antibodies drive myeloid activation and reprogram the tumor
- microenvironment through FcγR engagement and type I interferon signaling. Nat. Cancer 3, 1336-1350 (2022).
- Y. Zhang et al., Hijacking antibody-induced CTLA-4 lysosomal degradation for safer and more effective cancer immunotherapy. Cell Res. 29, 609-627 (2019).
- K. D. Lute et al., Human CTLA4 knock-in mice unravel the quantitative link between tumor immunity and autoimmunity induced by anti-CTLA-4 antibodies. Blood 106, 3127-3133 (2005).
- C. Schröter et al., A generic approach to engineer antibody pH-switches using combinatorial histidine scanning libraries and yeast display. MAbs 7, 138-151 (2015).
- K. K. Huynh, S. Grinstein, Regulation of vacuolar pH and its modulation by some microbial species. Microbiol. Mol. Biol. Rev. 71, 452-462 (2007).
- H. Stenmark, Rab GTPases as coordinators of vesicle traffic. Nat. Rev. Mol. Cell Biol. 10, 513-525 (2009)
- J. R. Goldenring, Recycling endosomes. Curr. Opin. Cell Biol. 35, 117-122 (2015).
- S. C. Oostindie, G. A. Lazar, J. Schuurman, P. Parren, Avidity in antibody effector functions and biotherapeutic drug design. *Nat. Rev. Drug Discov.* **21**, 715–735 (2022).
- S. I. Rudnick et al., Influence of affinity and antigen internalization on the uptake and penetration of Anti-HER2 antibodies in solid tumors. Cancer Res. 71, 2250-2259 (2011).
- L. S. Zuckier et al., Influence of affinity and antigen density on antibody localization in a modifiable 36. tumor targeting model. Cancer Res. 60, 7008-7013 (2000).
- A. Kretschmer, R. Schwanbeck, T. Valerius, T. Rösner, Antibody isotypes for tumor immunotherapy Transfus. Med. Hemother. 44, 320–326 (2017).
- A. D. Waldman, J. M. Fritz, M. J. Lenardo, A guide to cancer immunotherapy: From T cell basic science to clinical practice. Nat. Rev. Immunol. 20, 651-668 (2020).
- D. K. Challa, R. Velmurugan, R. J. Ober, E. Sally Ward, FcRn: From molecular interactions to regulation of IgG pharmacokinetics and functions. Curr. Top Microbiol. Immunol. 382, 249-272 (2014).
- X. Meng et al., FBXO38 mediates PD-1 ubiquitination and regulates anti-tumour immunity of T cells. Nature 564, 130-135 (2018).
- X. Wang et al., TOX promotes the exhaustion of antitumor CD8(+)T cells by preventing PD1 degradation in hepatocellular carcinoma. J. Hepatol. 71, 731-741 (2019).
- M. L. Burr et al., CMTM6 maintains the expression of PD-L1 and regulates anti-tumour immunity. Nature 549, 101-105 (2017).
- R. Mezzadra et al., Identification of CMTM6 and CMTM4 as PD-L1 protein regulators. Nature 549, 106-110 (2017).